Radiation efficiency of unbaffled and perforated plates near a rigid reflecting surface

A. Putra [a],*, D.J. Thompson [b]

[a] Faculty of Mechanical Engineering, Universiti Teknikal Malaysia Melaka, Hang Tuah Jaya 76100, Durian Tunggal, Malacca, Malaysia
[b] Institute of Sound and Vibration Research, University of Southampton, Highfield, Southampton SO17 1BJ, United Kingdom

ARTICLE INFO

ABSTRACT

The accurate prediction of sound radiation from plate-like structures remains a challenging problem. Although the case of a plate set in a rigid baffle can be solved analytically, when the plate radiates sound into free space the problem is more difficult to solve; nevertheless, several approaches have been proposed to determine the sound radiation from an unbaffled plate. The present study extends the consideration to the situation of an unbaffled plate which is located close to a rigid reflecting surface. For this purpose, Laulagnet's model for the radiation efficiency of an unbaffled plate is extended by modifying the Green's function to include an image source due to the reflecting surface. The results show that, depending on the distance between the plate and the rigid surface, the radiation efficiency is considerably reduced at low frequencies. Additional reduction of sound radiation can be achieved by introducing perforation to the plate. However, at higher frequencies, the radiation efficiency is amplified relative to that for the plate in the absence of the rigid surface, both with and without perforation. These results have also been validated experimentally.

1. Introduction

In many practical applications, a vibrating structure may be located near a rigid surface. For example, a machine may be installed close to a hard wall or floor. It is well known that a monopole source with constant volume velocity placed close to a rigid surface will radiate twice as much sound power as it does in a free field, due to the change in impedance loading [1]. A more complex case, which is nevertheless of fundamental importance, is the sound radiated by a vibrating flat plate located near a rigid surface. There appears to be a lack of suitable models to determine the sound radiation for such a situation.

Estimation of the sound radiation from vibrating plates and plate-like structures was proposed by Maidanik [2,3] for a rectangular plate set in an infinite baffle. Approximate formulae for frequency-average radiation efficiencies were given based on the assumption of equipartition of energy in the frequency band (and light damping). Wallace [4] derived the radiation efficiency for individual plate modes using the Rayleigh integral to calculate the total energy radiated to the farfield. Leppington et al. [5] also provided a detailed mathematical analysis of the radiation from modes of a simply supported panel as in terms of the acoustic wavenumber. Their results mostly agreed with the formulae of Maidanik [2], but a modified formula was given for the radiation close to the critical frequency. The results from Wallace were used by Xie et al. [6] to calculate the average radiation efficiency from the forced vibration of a plate as a summation over the contributions of individual modes.

---

* Corresponding author. Tel.: +606 234 6891; fax: +606 234 6884.
  E-mail address: azma.putra@utem.edu.my (A. Putra).

Schroter and Fahy [7] proposed a model for sound radiation from a baffled plate for a case where an infinite rigid surface is located close to the plate. It was found that, at low frequencies, the modal radiation efficiency is inversely proportional to the distance between the plate and the surface. At high frequencies, the radiation efficiency curve was found to fluctuate due to the acoustic 'cut-on' behaviour within the space between the plate (and its baffle) and the rigid surface.

For a similar case, Verheij et al. [8] investigated the sound radiation from a finite baffled plate into a shallow cavity and compared the radiation efficiency to that for a baffled plate radiating into a half-space. At low frequencies, where the cavity height is small compared with half the acoustic wavelength, the sound radiation is amplified, but when the height is greater than half the acoustic wavelength the average sound radiation is largely unaffected by the presence of the rigid surface. Numerical predictions using the finite element and boundary element methods were also carried out for a rib-stiffened plate with similar conclusions.

The problem of the radiation from an unbaffled plate is more difficult to solve as the velocity is known only over the surface of the plate, whereas in the remainder of the plane the pressure is known (zero) and the velocity is unknown. Various models have been published including analytical and semi-analytical methods to calculate the radiation from unbaffled plates [9–12]. The model proposed by Williams [9] was based on the FFT method [13] by using an iterative scheme in which the pressure in the source plane and then the particle velocity are determined from one another. It is found that there are convergence problems when finer resolution of sample spacing is used to calculate results for higher order modes. Atalla et al. [10] gave a numerical solution using the Kirchhoff–Helmholtz equation allowing the pressure to be defined anywhere within a volume enclosing the plate. A simplification was made where the pressure jump was neglected when calculating the velocity of the plate, allowing any boundary conditions to be derived analytically at the plate edges. The results showed that the unbaffled plate has a lower radiation efficiency compared with that of the baffled plate at low frequencies. However, there were found to be difficulties with the numerical implementation at high frequencies where the radiation efficiency of the unbaffled plate was overestimated.

Of particular interest is a model established by Laulagnet [12] which implemented the same technique as Atalla et al. [10] except that the pressure jump was taken into account and both velocity and pressure were expressed as a summation over plate modes. The radiation efficiency for a plate with simply supported edges was found to be lower than that in the baffled case; this difference reduces as the frequency increases. This method has been used by Putra and Thompson [14] to compare the average radiation efficiency of baffled and unbaffled plates for forced vibration.

Recently, Putra and Thompson [15] modified the Laulagnet's model [12] to consider the effect of introducing perforation in an unbaffled rectangular plate. The hole impedance was introduced to include the effect of perforation in terms of a continuously distributed surface impedance to represent the holes. This produces a model for the sound radiation from a perforated unbaffled plate. It was shown that the radiation efficiency reduces as the perforation ratio increases or as the hole size reduces.

The present study considers an unbaffled plate which is located close to a reflecting, rigid surface. The model is derived by extending Laulagnet's model [12] for the radiation efficiency of an unbaffled plate. An image source representing the presence of the reflecting surface can be introduced by modifying the Green's function [16]. This is then extended further by also introducing the impedance of holes into the formula in order to develop a model for a perforated unbaffled plate close to a rigid surface. Additionally, experimental results are presented for both solid and perforated plates close to a rigid surface.

2. Theory

2.1. Modification of Green's function

In this section a model is developed for the radiation from an unbaffled plate close to an infinite rigid surface, based on the model for radiation from an unbaffled plate established by Laulagnet [12].

Consider a situation, as shown in Fig. 1, in which an unbaffled, flat, thin vibrating plate of dimensions $a \times b$ with a surface area $S = ab$ is located at a distance D above an infinite rigid, reflecting surface lying in the xy-plane. On the rigid surface the normal fluid velocity is zero. This boundary condition is equivalent to the situation in which an imaginary plate, vibrating in the opposite direction, is located at a distance $2D$ below the real vibrating plate, in the absence of the infinite reflecting surface. The sound field below the rigid surface, of course, has no physical meaning. However, the corresponding sound field above the rigid surface ($z \geq 0$) includes the reflected field from this surface.

Assume that the plate is excited by harmonic force distribution $F(x,y)$ of angular frequency ω. Moreover, $\Delta p(x,y)$ is the difference between the acoustic surface pressure on the two sides of the plate defined as

$$\Delta p(x,y) = p^-(x,y) - p^+(x,y) \tag{1}$$

where p^- is the pressure directly below the plate and p^+ is the pressure above it. The equation of motion of the plate is given by [12]

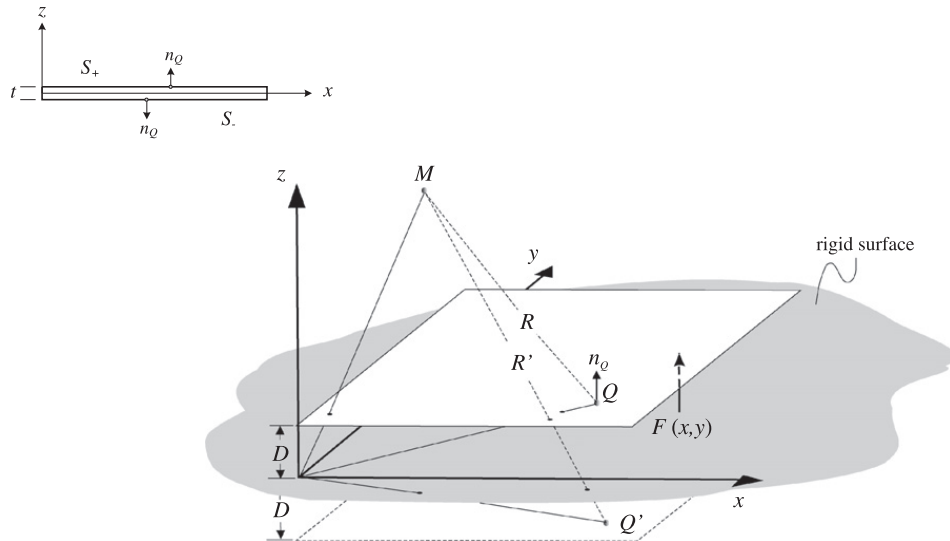$$\frac{B}{j\omega} \nabla^4 v(x,y) + jm_s\omega v(x,y) = F(x,y) + \Delta p(x,y) \tag{2}$$

Fig. 1. A simply supported plate in a medium and located at a distance D from an infinite rigid surface.

where $B = Et^3/12(1-v^2)$ is the plate bending stiffness, in which E is Young's modulus, t is the plate thickness and v is Poisson's ratio, m_s is the mass per unit area, $v(x,y)$ is the transverse velocity of the plate and $\nabla^4 = \partial^4/\partial x^4 + 2\partial^4/(\partial x^2 \partial y^2) + \partial^4/\partial y^4$. The effect of damping can be included by replacing the plate bending stiffness B by $B(1+j\eta)$ where η is the damping loss factor.

For a vibrating surface S_v located in the free field, the pressure at a point M in the fluid can be obtained by using the Kirchhoff–Helmholtz (K–H) integral [17]

$$p(M) = \int_{S_v} \left(p(Q) \frac{\partial G(Q,M)}{\partial n_Q} - G(Q,M) \frac{\partial p}{\partial n_Q} \right) dS_v \tag{3}$$

where Q is a point on the plate surface S_v and G is the free-field Green's function. The integral is performed over both sides of the plate. In Eq. (3), the first and second terms correspond to the dipole and monopole source radiation, respectively.

The Green's function can now be modified [16] to include the contribution of the image source $Q' = (x,y,-z)$ to the pressure at the field point $M = (x_0,y_0,z_0)$, giving

$$G(Q,M) = \frac{e^{-jkR}}{4\pi R} + \frac{e^{-jkR'}}{4\pi R'} \tag{4}$$

where $k = \omega/c$ is the acoustic wavenumber, c is the speed of sound, $R = ((x_0-x)^2 + (y_0-y)^2 + (z_0-z)^2)^{1/2}$ and $R' = ((x_0-x)^2 + (y_0-y)^2 + (z_0+z)^2)^{1/2}$. The Green's function must satisfy

$$\nabla^2 G(Q,M) + k^2 G(Q,M) = \delta(x_0-x)\delta(y_0-y)\delta(z_0-z) + \delta(x_0-x)\delta(y_0-y)\delta(z_0+z) \tag{5}$$

Taking the two-dimensional Fourier transform of Eq. (5), the Green's function can be expressed as [18]

$$G = \frac{j}{8\pi^2} \int_{-\infty}^{\infty} \int_{-\infty}^{\infty} \frac{1}{k_z} \{e^{jk_z|z-z_0|} + e^{jk_z(z+z_0)}\} e^{jk_x(x-x_0)} e^{jk_y(y-y_0)} \, dk_x \, dk_y \tag{6}$$

where $k_z = (k^2 - k_x^2 - k_y^2)^{1/2}$. $Q = (x,y,z)$ is now chosen to be a point on the plate surface ($z=D$), while $M = (x_0,y_0,z_0)$ is a field point. Attention is limited to positions M above the plate (in the half space $z_0 \geq z$). The second term within the brackets is the image source contribution. For $z_0 \geq z$, the terms in the brackets can be expressed as

$$e^{jk_z(z_0-z)} + e^{jk_z(z+z_0)} = 2e^{jk_z z_0} \cos(k_z z) \tag{7}$$

while for $z_0 \leq z$ the terms z_0 and z in Eq. (7) should be exchanged.

Since the plate thickness is assumed to be very small, the normal velocity is identical on the plate surfaces S_+ and S_- and hence $\partial p/\partial z_Q$ is equal on both sides of the plate. However, the sign of the normal vector $\mathbf{n}_Q$ is reversed so that the second term in Eq. (3) is zero. Thus by performing the integration over the plate surfaces, Eq. (3) reduces to

$$p(M)|_{z=D} = -\int_S \Delta p \frac{\partial G(Q,M)}{\partial z_Q} dS \tag{8}$$

where $S = S_+$ is the area of the plate. This leaves only the dipole term.

Applying Euler's equation ($\partial p/\partial z = -j\rho\omega v$) in the plane of the plate at $z=D$ in Eq. (8) and substituting Δp from the equation of motion in Eq. (2) yields

$$-j\rho\omega v(M) = -\int_S \left(\frac{B}{j\omega}\nabla^4 v(Q) + jm_s\omega v(Q) - F(Q)\right)\frac{\partial^2 G(Q,M)}{\partial z_Q \, \partial z_M}\,dS \tag{9}$$

2.2. Velocity and force excitation in terms of modal series

The plate velocity can be considered as a summation over plate modes (m,n) which can be written as

$$v(x,y) = \sum_{m=1}^{\infty}\sum_{n=1}^{\infty} u_{mn}\varphi_{mn}(x,y) \tag{10}$$

where u_{mn} is the modal complex velocity amplitude and φ_{mn} is the mode shape function. For simplicity the case of a simply supported plate with dimensions $a \times b$ is taken. The mode shape φ_{mn} is then the product of two sinusoidal functions, i.e.

$$\varphi_{mn}(x,y) = \sin\left(\frac{m\pi x}{a}\right)\sin\left(\frac{n\pi y}{b}\right) \tag{11}$$

Here it is assumed that the individual modes are excited simultaneously and with equal energy [19]. The same expansion is also applied to the excitation force F which is written as [12]

$$F(x,y) = \sum_{m=1}^{\infty}\sum_{n=1}^{\infty} F_{mn}\varphi_{mn}(x,y) \tag{12}$$

where F_{mn} is the modal force amplitude. This series expansion for the external force term allows the regularisation of the numerical results since the series will be limited to the same mode order, both for the force and the velocity. Otherwise, the results will be numerically unstable.

Substituting Eqs. (10) and (12) into Eq. (9) gives

$$\rho\omega^2\sum_{m=1}^{\infty}\sum_{n=1}^{\infty} u_{mn}\varphi_{mn}(x_0,y_0) = -\int_S\sum_{m=1}^{\infty}\sum_{n=1}^{\infty}(m_s(\omega_{mn}^2 - \omega^2)u_{mn} - j\omega F_{mn})\varphi_{mn}(x,y)\frac{\partial^2 G(Q,M)}{\partial z_Q \, \partial z_M}\,dS \tag{13}$$

where $\omega_{mn} = (B/m_s)^{1/2}[(m\pi/a)^2 + (n\pi/b)^2]$ is the natural frequency of mode (m,n).

2.3. Acoustic cross-modal coupling terms

This section defines the matrix of the so-called acoustical cross-modal coupling terms. The orthogonality relationship with mode (p,q) for a simply supported uniform plate gives

$$\int_S \varphi_{mn}\varphi_{pq}\,dS = (S/4)\delta_{mp}\delta_{nq} \tag{14}$$

where δ_{mp} is the Kronecker delta. Implementing Eq. (14), after multiplying Eq. (13) by φ_{pq} and integrating over the plate area gives

$$\rho\omega^2\left(\frac{S}{4}\right)u_{pq} = \sum_{m=1}^{\infty}\sum_{n=1}^{\infty}\{j\omega F_{mn} - m_s(\omega_{mn}^2 - \omega^2)u_{mn}\}C_{pqmn} \tag{15}$$

where $C_{pqmn} = C_{mnpq}$ are the acoustical cross-modal coupling terms [12]:

$$C_{pqmn} = \int_S\int_S \varphi_{pq}(x_0,y_0)\frac{\partial^2 G}{\partial z\,\partial z_0}(x,x_0,y,y_0,z=z_0=D)\varphi_{mn}(x,y)\,dx\,dy\,dx_0\,dy_0 \tag{16}$$

Substituting the half-space Green's function from Eq. (4) into Eq. (16) and performing the two integrals over S yields

$$C_{pqmn} = \frac{1}{4\pi^2}\int_{-\infty}^{\infty}\int_{-\infty}^{\infty} k_z\,e^{jk_z z_0}\sin(k_z z)\tilde{\varphi}_{pq}^*(k_x,k_y)\tilde{\varphi}_{mn}(k_x,k_y)\,dk_x\,dk_y \tag{17}$$

where $\tilde{\varphi}_{mn}$ is the Fourier transform of the mode shape φ_{mn}, which for simply supported edges is given by [12]

$$\tilde{\varphi}_{mn}(k_x,k_y) = \frac{ab}{\pi^2 mn}\left[\frac{(-1)^m e^{-j\mu}-1}{(\mu/(m\pi))^2-1}\right]\left[\frac{(-1)^n e^{-j\chi}-1}{(\chi/(n\pi))^2-1}\right] \tag{18}$$

where $\mu = k_x a$ and $\chi = k_y b$. For $z = z_0 = D$, after algebraic manipulation, Eq. (17) becomes

$$C_{pqmn} = C_{mnpq} = \frac{4}{pqmn}\left(\frac{ab}{\pi^3}\right)^2\int_0^{\infty}\int_0^{\infty} k_z e^{jk_z D}\sin(k_z D)\,\Upsilon\Omega\,dk_x\,dk_y \tag{19}$$

where

$$\Upsilon = \frac{1-(-1)^p \cos\mu}{((\mu/p\pi)^2-1)((\mu/m\pi)^2-1)}, \quad \Omega = \frac{1-(-1)^q \cos\chi}{((\chi/q\pi)^2-1)((\chi/n\pi)^2-1)} \tag{20}$$

The lower limit of integration has been changed from $-\infty$ to 0 by making use of the fact that the integrand is an even function with respect to k_x when the mode orders (p,m) are of the same parity. Similarly, with respect to k_y, the integrand is an even function when the mode orders (q,n) are of the same parity. The remaining cases will have $C_{pqmn} = 0$.

After re-arranging Eq. (15), it can be written in matrix form as

$$m_s \mathbf{C}(\mathbf{A}-\mathbf{I}\omega^2)\mathbf{u}+\rho\omega^2\left(\frac{S}{4}\right)\mathbf{u} = j\omega \mathbf{CF} \tag{21}$$

where $\mathbf{C}$ is the matrix of complex acoustic coupling terms C_{pqmn}, $\mathbf{u}$ is the vector of modal velocities u_{mn}, $\mathbf{F}$ is the vector of modal excitation forces F_{mn}, $\mathbf{I}$ is the identity matrix and $\mathbf{A}$ is a diagonal matrix of squared natural frequencies:

$$\mathbf{A} = \begin{bmatrix} \omega_{11}^2 & 0 & \cdots & 0 \\ 0 & \omega_{12}^2 & \cdots & \vdots \\ \vdots & \vdots & \ddots & \vdots \\ 0 & \cdots & \cdots & \omega_{mn}^2 \end{bmatrix} \tag{22}$$

Multiplying Eq. (21) by $\mathbf{C}^{-1}$, i.e. the inverse of matrix $\mathbf{C}$, yields

$$m_s(\mathbf{A}-\mathbf{I}\omega^2)\mathbf{u}+\rho\omega^2\left(\frac{S}{4}\right)\mathbf{C}^{-1}\mathbf{u} = j\omega \mathbf{F} \tag{23}$$

Eq. (23) can be simplified by making the approximation of retaining only the self-modal coupling terms of Eq. (19). The inverse of the cross-modal coupling terms $\mathbf{C}^{-1}$ can then be replaced by a diagonal matrix of terms $1/C_{pqpq}$. This approximation has been found to work well for an unbaffled plate immersed in a light fluid such as air [12,16], particularly for the case considered involving an average over all possible force positions.

By thus neglecting the cross-modal coupling contributions in the sound radiation, Eq. (23) can be approximated by

$$M_{pq}(\omega_{pq}^2-\omega^2)u_{pq}+\rho\omega^2\left(\frac{S}{4}\right)^2\left(\frac{1}{C_{pqpq}}\right)u_{pq} = j\omega\left(\frac{S}{4}\right)F_{pq} \tag{24}$$

where $M_{pq} = m_s(S/4)$ is the generalized mass for mode (p,q). Eq. (24) can be solved for each mode separately to find the modal complex velocity amplitude u_{pq}.

2.4. Introducing perforation

It is now of interest to extend the above model for a vibrating plate close to an infinite rigid surface to allow the vibrating plate to be perforated. A model for the radiation efficiency of a perforated unbaffled plate has been proposed by Putra and Thompson [15]. This was also derived from Laulagnet's model for a solid unbaffled plate, in this case by introducing a surface impedance representing a distribution of holes on the plate. This is here extended to the case where the vibrating plate is close to a rigid surface.

In the presence of a distribution of holes in a plate, the particle velocity on the plate surface is modified by the fluid flow across the holes v_f. The net particle velocity $\overline{v}$ formed by the combination of the normal velocity of the plate v and the fluid motion v_f is given by [20]

$$\overline{v} = v(1-\tau)+v_f \tag{25}$$

where τ is the perforation ratio. For a perforated plate with holes that are close together relative to the acoustic wavelength, these can be considered as continuously distributed. The equivalent fluid velocity through the holes averaged locally over the plate area will be $v_f = \tau v_h$ in which v_h is the flow velocity through a single hole in a plate. This can be given by

$$v_h = \frac{\Delta p}{Z_h} \tag{26}$$

where Z_h is the impedance of hole and Δp is the pressure difference as given in Eq. (1). Thus the specific acoustic impedance of the distribution of holes will be $z_h = Z_h/\tau$. This can also be written as [15]

$$z_h = \frac{j\rho ck}{\tau}\left[t+\left(\frac{8}{3\pi}\right)d_o\right] \tag{27}$$

where d_o is the hole diameter. The hole impedance in Eq. (27) is derived from a circular tube with length t proposed by Maa [21]. In Eq. (27) the resistive part of the hole impedance Z_h has been neglected; the model could readily be extended to include this term but it can be neglected for holes with diameter greater than about 1 mm [15].

By introducing perforation, the equation of motion (Eq. (2)) is modified to

$$\frac{B}{j\omega}\nabla^4 v(x,y) + jm_s\omega v(x,y) = F(x,y) + (1-\tau)\Delta p(x,y) \tag{28}$$

Substituting the mean particle velocity $\overline{v}$ from Eq. (25) in place of the velocity v in the left-hand side of Eq. (9) gives

$$-j\rho\omega(1-\tau)^2 v(M) - \frac{j\rho\omega}{z_h}\left(\frac{B}{j\omega}\nabla^4 v(M) + jm_s\omega v(M) - F(M)\right)$$
$$= -\int_S \left(\frac{B}{j\omega}\nabla^4 v(Q) + jm_s\omega v(Q) - F(Q)\right)\frac{\partial^2 G(Q,M)}{\partial z_Q\,\partial z_M}\,dS \tag{29}$$

Performing the same procedure as in Sections 2.1.1 and 2.1.2, the matrix form as in Eq. (23) is now given by

$$m_s(\mathbf{A}-\mathbf{I}\omega^2)\mathbf{u} + \rho\omega^2\left(\frac{S}{4}\right)\mathbf{C}^{-1}\left((1-\tau)^2\mathbf{I} - \frac{jm_s}{\omega z_h}(\mathbf{A}-\mathbf{I}\omega^2)\right)\mathbf{u} = \left(j\omega\mathbf{I} + \frac{\rho\omega^2}{z_h}\left(\frac{S}{4}\right)\mathbf{C}^{-1}\right)\mathbf{F} \tag{30}$$

Again, by neglecting the cross-modal coupling terms, Eq. (30) can be expressed in uncoupled form as

$$M_{pq}(\omega_{pq}^2-\omega^2)u_{pq} + \rho\omega^2\left(\frac{S}{4}\right)^2\left(\frac{1}{C_{pqpq}}\right)\left((1-\tau)^2 - \frac{4jM_{pq}}{S\omega z_h}(\omega_{pq}^2-\omega^2)\right)u_{pq} = \left(j\omega + \frac{\rho\omega^2}{z_h}\left(\frac{S}{4}\right)\frac{1}{C_{pqpq}}\right)\left(\frac{S}{4}\right)F_{pq} \tag{31}$$

The case of a solid plate as in Eq. (24) can be recovered by introducing a very large value of z_h and setting $\tau = 0$.

2.5. Sound power and radiation efficiency

In Laulagnet's model [12] the sound power radiated by an unbaffled plate is calculated by defining the pressure difference across the plate in terms of a series of plate modes as well as the velocity amplitude. Having obtained the velocity amplitude u_{pq} from Eq. (24) or Eq. (31), the radiated sound power for each mode (p,q) can be calculated by [15]

$$W_{pq} = \frac{S}{8(1-\tau)}\mathrm{Re}\left\{\left(F_{pq} + \frac{jm_s}{\omega}(\omega_{pq}^2-\omega^2)u_{pq}\right)u_{pq}^*\right\} \tag{32}$$

where $\tau = 0$ for the solid plate, $*$ indicates complex conjugate and use has been made of orthogonality of the modes.

The overall radiation efficiency can be calculated from a summation of all modal components [6,15]

$$\sigma = \frac{\sum_{p=1}^\infty\sum_{q=1}^\infty W_{pq}}{\rho c(2ab)(1-\tau)\sum_{p=1}^\infty\sum_{q=1}^\infty \overline{\langle|v_{pq}|^2\rangle}} \tag{33}$$

where $\overline{\langle|v_{pq}|^2\rangle}$ is the spatially averaged squared velocity amplitude of mode (p,q). For a simply supported plate this is given by

$$\overline{\langle|v_{pq}|^2\rangle} = \frac{|u_{pq}|^2}{4} \tag{34}$$

where u_{pq} is the modal amplitude, given in Eq. (10). The overbar indicates that this has been averaged over all possible forcing locations (x_0,y_0). The radiation efficiency of the unbaffled plate takes into account the fluid loading on both sides of the plate. Note that the total surface area of the $2ab$ has been used in the denominator of Eq. (33). Again, the perforation ratio τ in Eq. (33) should be set to zero for the solid panel.

3. Radiation efficiency and the effect of rigid surface

3.1. Results for solid plates

Fig. 2 shows the modal radiation efficiencies of a solid (unperforated) aluminium plate ($E = 7.1 \times 10^{10}$ N/m^2, $\rho_s = 2700$ kg/m^3, $v = 0.33$) for different modes and different distances D from a rigid surface, together with the equivalent results for the case without the rigid surface. The plate dimensions are taken as $0.65 \times 0.5 \times 0.003$ m, with $\eta = 0.1$. The plate is excited by a unit point force, with the results representing the average over force positions across the plate surface.

For each mode shape (m,n), a modal coincidence frequency can be identified, given by $k^2 = (m\pi/a)^2 + (n\pi/b)^2$. In each case the modal radiation efficiency of the unbaffled plate rises to a peak at this frequency, above which it tends to unity. The slope of the radiation efficiency curve below this frequency is between 40 and 80 dB/decade, depending on the mode order, see [15]. For the plate close to the rigid surface this slope is, in each case, 20 dB/decade steeper than without the rigid surface. For example, for mode (1,1), the unbaffled plate corresponds to a dipole source whereas, close to the rigid surface, the image source results in the formation of a quadrupole source.

With the introduction of the rigid surface, a much sharper peak occurs for each mode at around the modal coincidence frequency. The peak can be seen to occur at the same frequency for different distances, D. This peak is caused by the formation of an acoustic standing wave between the plate and the rigid surface in the direction parallel to the plate. Some smaller peaks also occur at higher frequencies for higher order modes.
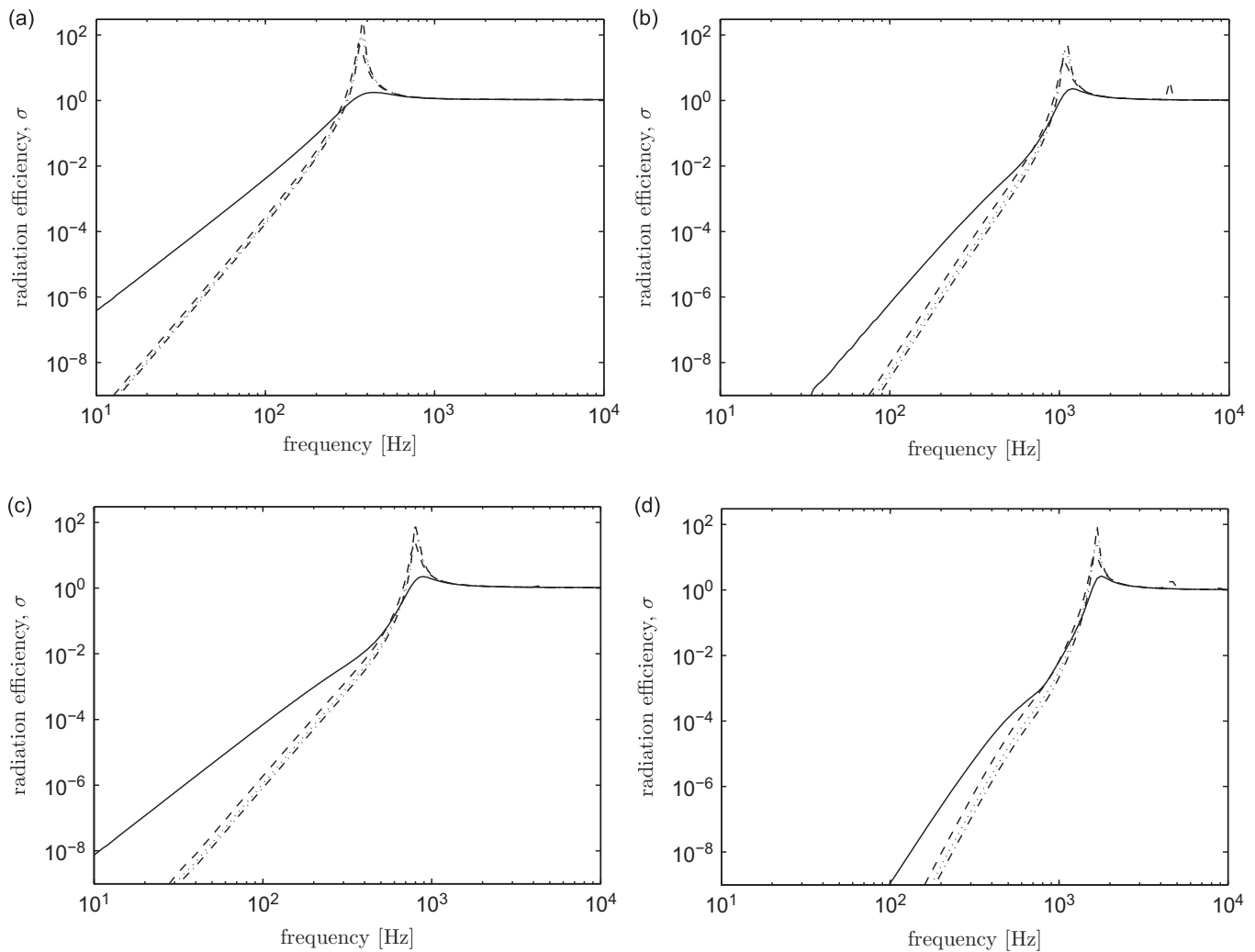
Fig. 2. Radiation efficiency of an unbaffled plate near a rigid surface for (a) mode (1,1), (b) mode (2,3), (c) mode (3,1) and (d) mode (4,4): —, absence of rigid surface; –, $D=40$ mm; $\cdots$, $D=20$ mm; $-\cdot-$, $D=10$ mm (aluminium plate, $0.65 \times 0.5 \times 0.003$ m).

Fig. 3 shows the modal radiation efficiencies and the total radiation efficiency for the unbaffled plate located 20 and 40 mm above the rigid surface. To obtain accurate results up to 10 kHz, the radiation efficiencies were calculated for all modes up to order $m=25$ in the x direction and order $n=20$ in the y direction. It can be seen that below 100 Hz, the average radiation efficiency has a frequency dependence of 60 dB/decade, which is dominated by the contribution of mode (1,1), as shown in Fig. 2(a). This shows that at very low frequency the vibrating plate behaves like a quadrupole source, a very inefficient radiator. However, this requires that the distance from the rigid surface is very small compared with the acoustic wavelength ($kD \ll 1$).

In Fig. 3 very high peaks can be seen in the modal radiation efficiencies at very high frequencies. These appear to be due to a standing wave effect in the height direction when the distance between the plate and the rigid surface is a multiple of half the acoustic wavelength ($kD = n\pi$ with n a positive integer). Thus these high peaks in the modal radiation efficiency start at 8.5 kHz for $D=20$ mm and at 4.2 kHz for $D=40$ mm with a further set of peaks at 8.5 kHz. These peaks effectively also lead to a broad peak in the total radiation efficiency above the critical frequency, as seen in Fig. 3(b) at around 7 kHz.

Fig. 4(a) shows the total radiation efficiency for the unbaffled plate located close to a rigid surface compared with that for the plate without the rigid surface. Again, for frequencies below the fundamental resonance frequency (which occurs at 70 Hz), the radiated sound is reduced as the vibrating plate is brought closer to the rigid wall. However, for frequencies above about 250 Hz the radiation is increased by the presence of the rigid surface. This corresponds to the standing waves between the plate and the rigid surface, responsible for the peaks in the modal radiation efficiencies. Fig. 4(b) shows similar phenomena for a plate with different dimensions and thickness where the increase occurs above about 500 Hz. This increased radiation occurs when half the acoustic wavelength is smaller than the plate dimensions and is similar to the amplification found for the baffled plate case [7,8].

The effect of the rigid surface on the radiated sound power (or radiation efficiency) can be represented quantitatively in dB by the insertion gain [15]

$$\Pi = 10\log_{10}\left(\frac{\sigma_{rs}}{\sigma}\right) \tag{35}$$
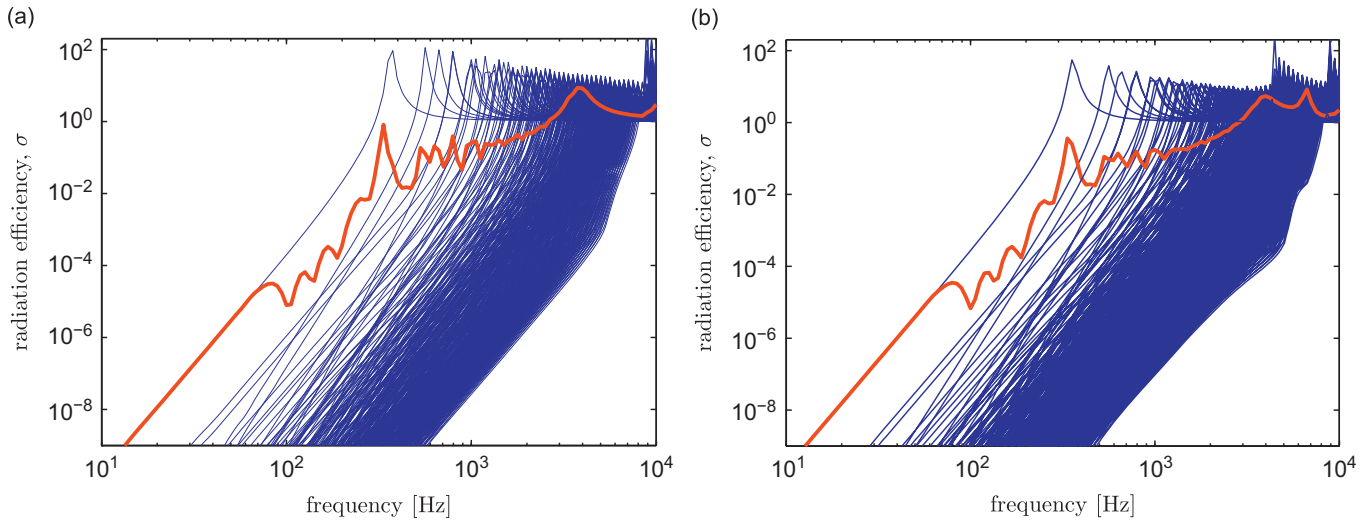
(a)

(b)

Fig. 3. Modal radiation efficiency (thin lines) and total radiation efficiency (thick line) of an unbaffled plate near rigid surface: (a) $D=20$ mm and (b) $D=40$ mm (aluminium plate, $0.65 \times 0.5 \times 0.003$ m, $\eta=0.1$).
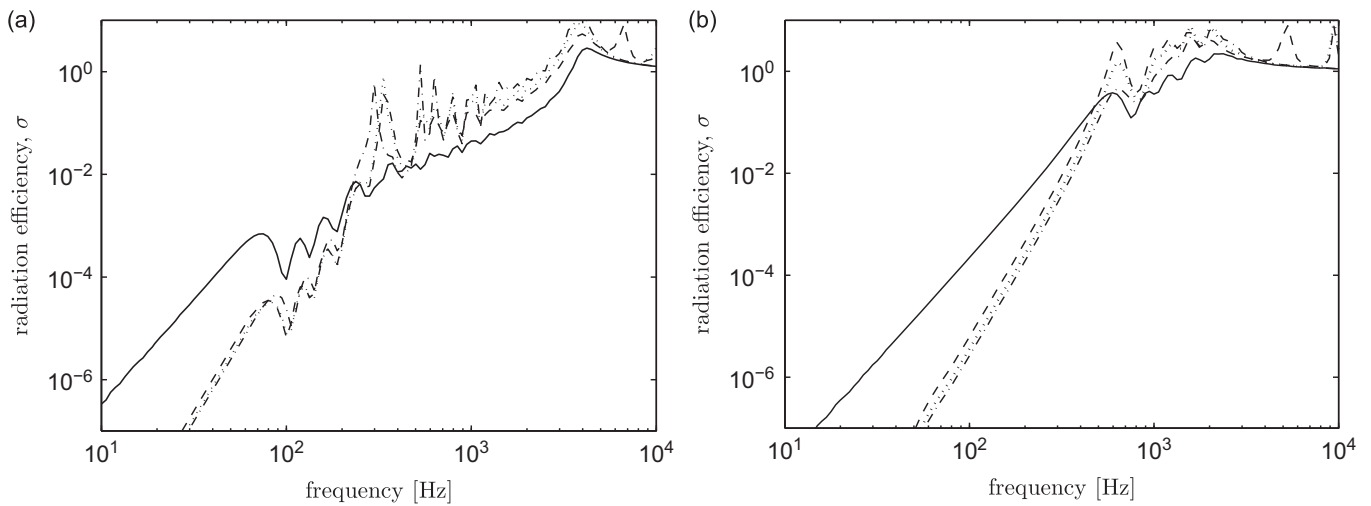
(a)

(b)

Fig. 4. Radiation efficiency of an unbaffled plate near a rigid surface, $\eta=0.1$; (a) $0.65 \times 0.5 \times 0.003$ m and (b) $0.325 \times 0.25 \times 0.006$ m: —, without rigid surface; –, $D=40$ mm; $\cdots$, $D=20$ mm; $-\cdot-$, $D=10$ mm.

where σ_{rs} is the radiation efficiency of a plate near a rigid surface and σ is the result for a plate with no rigid surface. Fig. 5 shows this insertion gain from the results in Fig. 4. For both sets of plate dimensions, it is clear that the radiated sound power is reduced considerably at low frequencies, particularly below the fundamental resonance frequency. Here, the insertion gain reduces by about 1 dB for a halving of the distance D. Above about 1 kHz the sound power increases by an average of 5–6 dB for $D=10$ mm; this corresponds to the edge mode region of radiation [3,17]. The insertion gain in this region is increased by 1 dB when the distance from the rigid surface is halved. The insertion gain decreases rapidly above the critical frequency (4 kHz for the 3 mm plate and 2 kHz for the 6 mm plate) although there are additional peaks for close distances, as noted above.

3.2. Results for perforated plates

Fig. 6 plots the modal radiation efficiencies and the total radiation efficiency for an example perforated plate having hole diameter of 10 mm and 10 percent perforation ratio. Apart from this the plate has the same dimensions and properties as the solid plate considered in the previous section. The plate is again placed 20 or 40 mm above the rigid surface. As in Fig. 3 strong peaks occur at high frequency (>4.2 kHz) when half the acoustic wavelength is less than the distance D. However, the sharp peaks found previously at the modal coincidence frequencies above 350 Hz have now vanished. Thus the perforation prevents the formation of these standing waves between the vibrating plate and the rigid surface.

Fig. 7 compares the total radiation efficiencies for solid and perforated plates for distances of 10, 20 and 40 mm from a rigid surface and for two different plate sizes. It can be seen clearly here that the peaks occurring for the solid plate below the critical frequency have completely vanished for the perforated plate. For both plate sizes considered, the reduction due
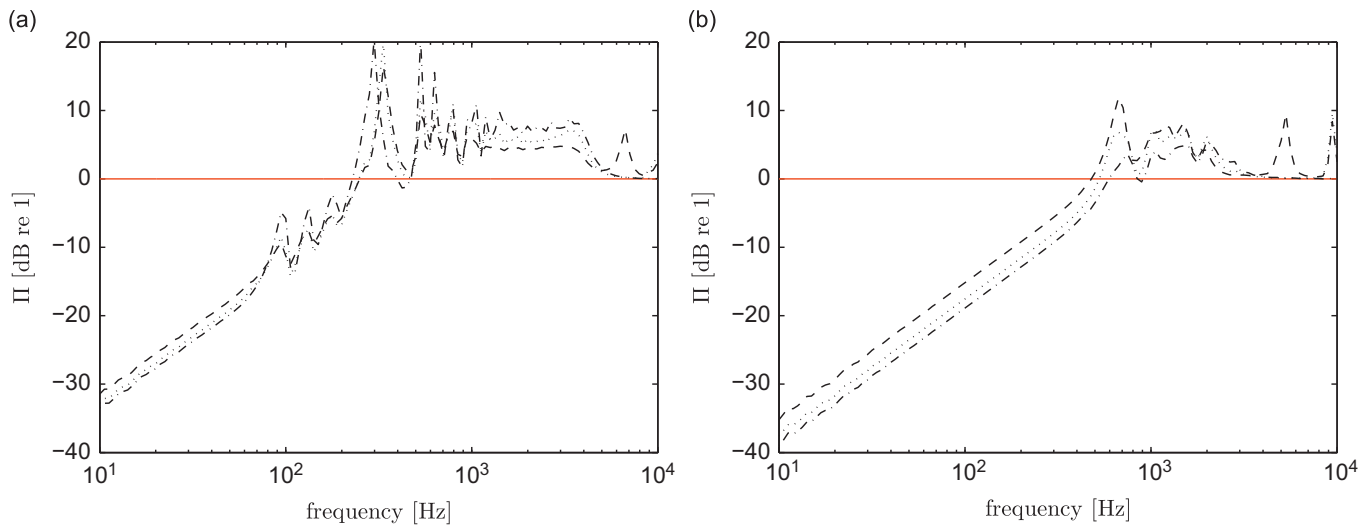
Fig. 5. Insertion gain due to the introduction of a rigid surface for radiated sound power from an unbaffled plate (a) $0.65 \times 0.5 \times 0.003$ m and (b) $0.325 \times 0.25 \times 0.006$ m; $\eta = 0.1$: –, $D=40$ mm; $\cdots$, $D=20$ mm; $-\cdot-$, $D=10$ mm.
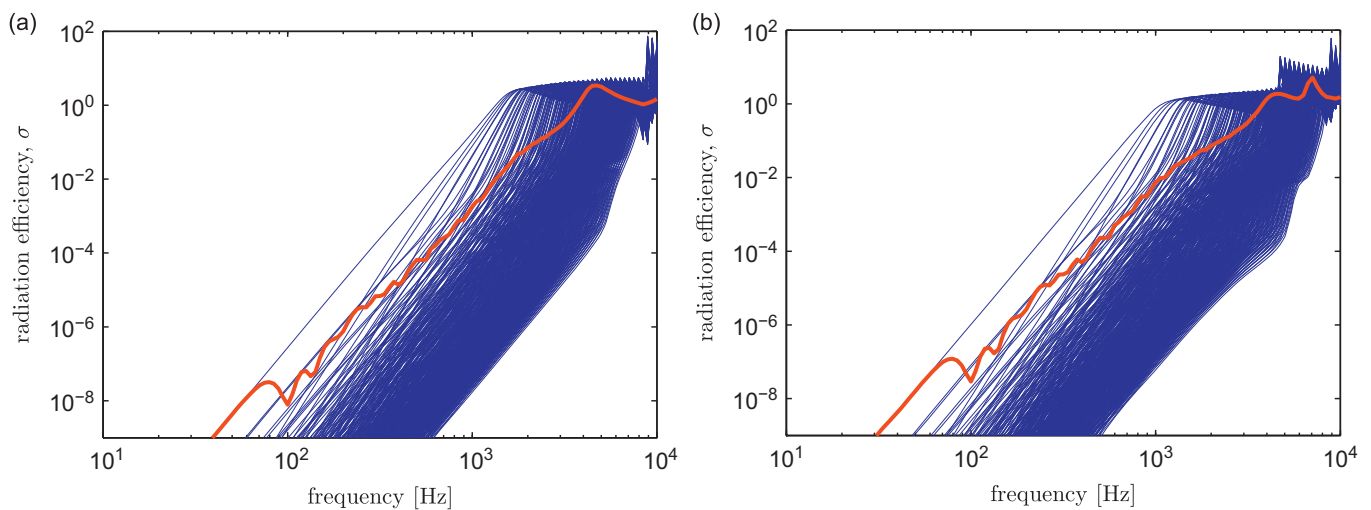

Fig. 6. Modal radiation efficiency (thin lines) and total radiation efficiency (thick line) of a perforated unbaffled plate near rigid surface: (a) $D=20$ mm and (b) $D=40$ mm (aluminium plate, $0.65 \times 0.5 \times 0.003$ m, $\eta = 0.1$, $d_o=10$ mm, $\tau = 10$ percent).

to perforation is effective over a wide range of frequency, up to the critical frequency (4 and 2 kHz respectively), as also found in the case without the presence of the rigid surface [15].

Fig. 8 shows the total radiation efficiency of a perforated plate for different distances from a rigid surface and for two different plate sizes, together with the radiation efficiency of the same plate in the absence of the rigid surface. As for the solid plates, a substantial reduction can be seen at low frequencies and amplification of the results at high frequencies. However, compared with the results from solid plates in Fig. 4, the effect of varying the distance from the rigid surface is greater for a perforated plate. This can be seen clearly in Fig. 9, showing the insertion gain due to the rigid surface for the perforated plate. A significant reduction of the radiated sound can be seen for frequencies below the fundamental resonance frequency. In this region the level now reduces by 5 dB for each halving of the distance from the rigid surface compared with only 1 dB for the case of the solid plate. The amplification of the sound power (seen as fluctuations) in the corner mode region, for instance in the region 200–1 kHz in Fig. 5(a) for the solid plate case, is now reduced considerably for the case of a perforated plate. The amplification begins in the edge mode region and extends up to the critical frequency; in this region the sound power increases by roughly 5 dB.

4. Experimental validation

4.1. Experimental arrangement

Measurements have been conducted to determine the radiation efficiency of a number of unperforated plates with 1.5 and 3 mm plate thickness and corresponding perforated plates with varying perforation ratios. As is clear from Eq. (33), the
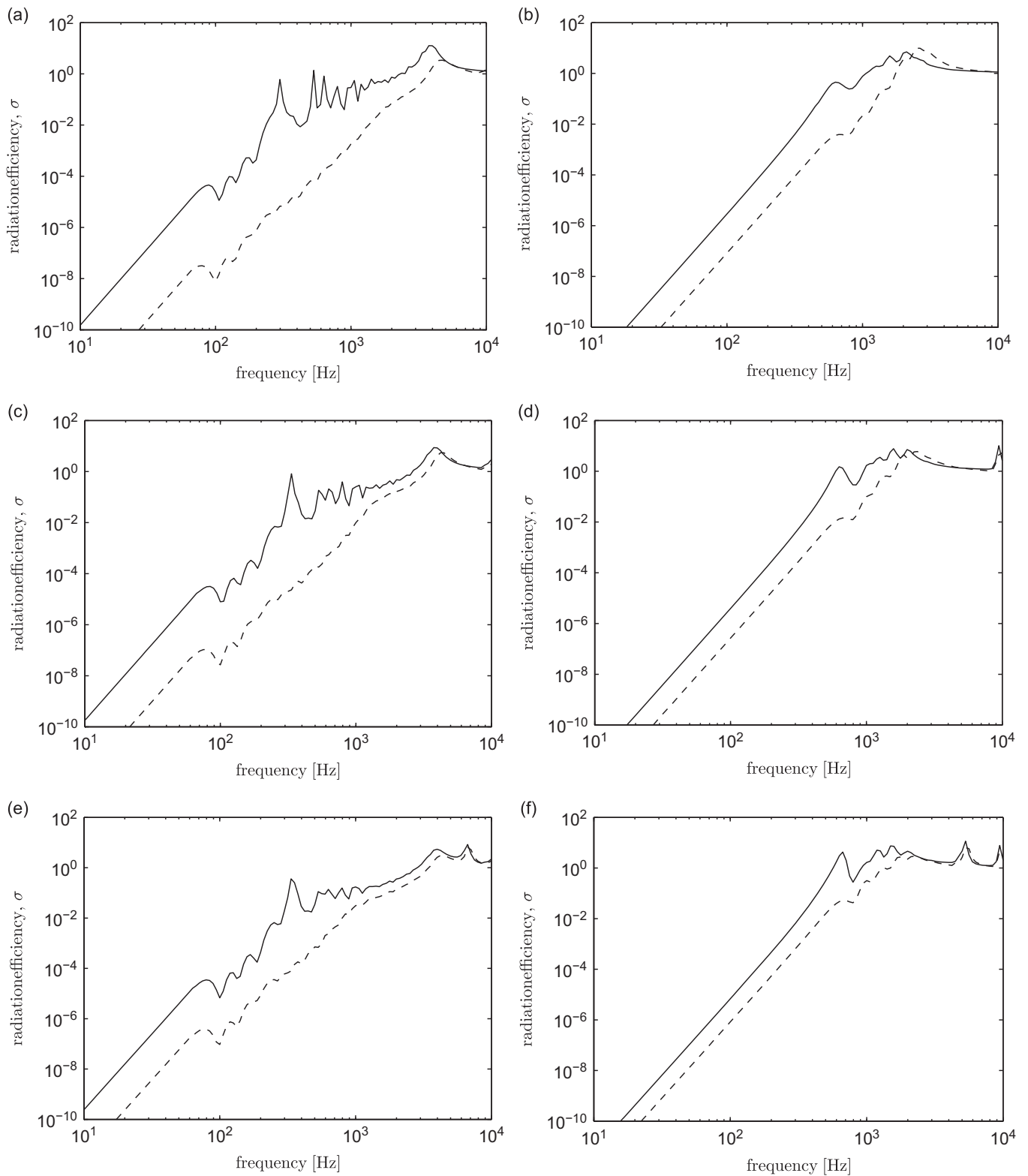
A. Putra, D.J. Thompson / Journal of Sound and Vibration 330 (2011) 5443–5459

Fig. 7. Radiation efficiency of a perforated unbaffled plate near rigid surface: —, solid; –, perforated; (a), (b) $D=10$ mm, (c), (d) $D=20$ mm and (e), (f) $D=40$ mm ($d_o=10$ mm, $\tau=10$ percent, $\eta=0.1$; left column: $0.65\times0.5\times0.003$ m, right column: $0.325\times0.25\times0.006$ m).

experiment requires mechanical measurements to obtain the spatially averaged squared velocity $\overline{\langle|v_{mn}|^2\rangle}$ and also acoustical measurements for the radiated sound power W. Both quantities have been determined for a unit force.

The realization of an ideal simply supported boundary condition in practice is not easy. For practical reasons, the plate was supported on a soft pieces of foam placed under each corner of the plate on the floor of the reverberant chamber. This produced effectively free-free boundary conditions. The thicknesses of the foam used were 10, 20 and 40 mm. This thickness thus becomes the distance D of the plate from the rigid surface. The arrangement is shown in Fig. 10. To obtain
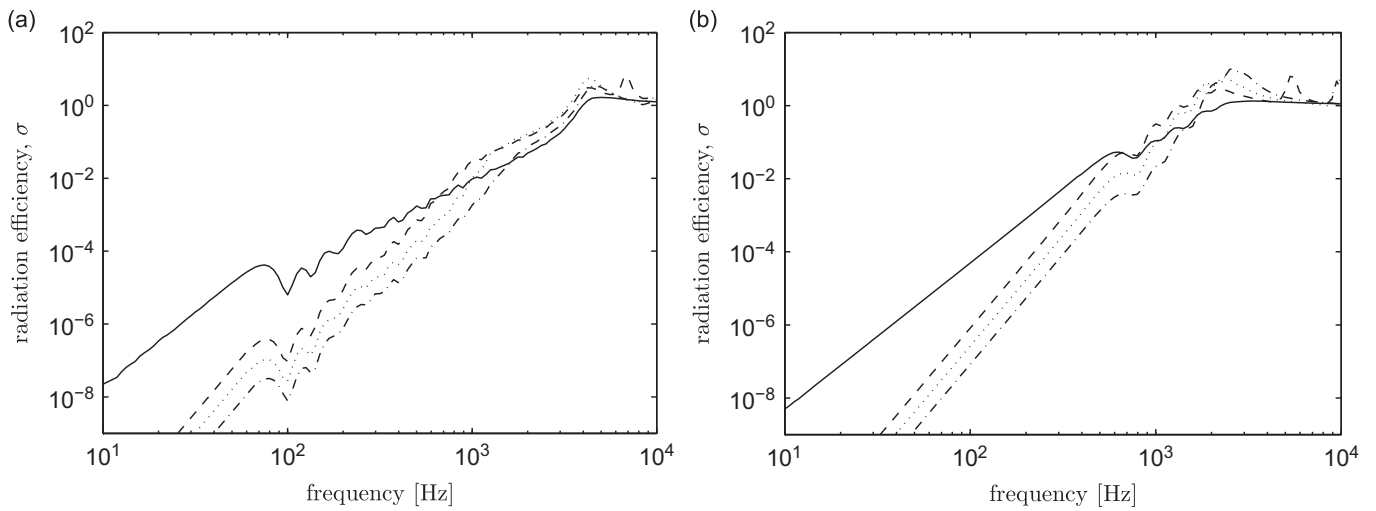
Fig. 8. Radiation efficiency of perforated unbaffled plate near rigid surface: —, absence of rigid surface; –, $D=40$ mm; $\cdots$, $D=20$ mm; $-\cdot-$, $D=10$ mm. Aluminium plate with $\eta=0.1$, $d_o=10$ mm, $\tau=10$ percent. (a) $0.65 \times 0.5 \times 0.003$ m and (b) $0.325 \times 0.25 \times 0.006$ m.
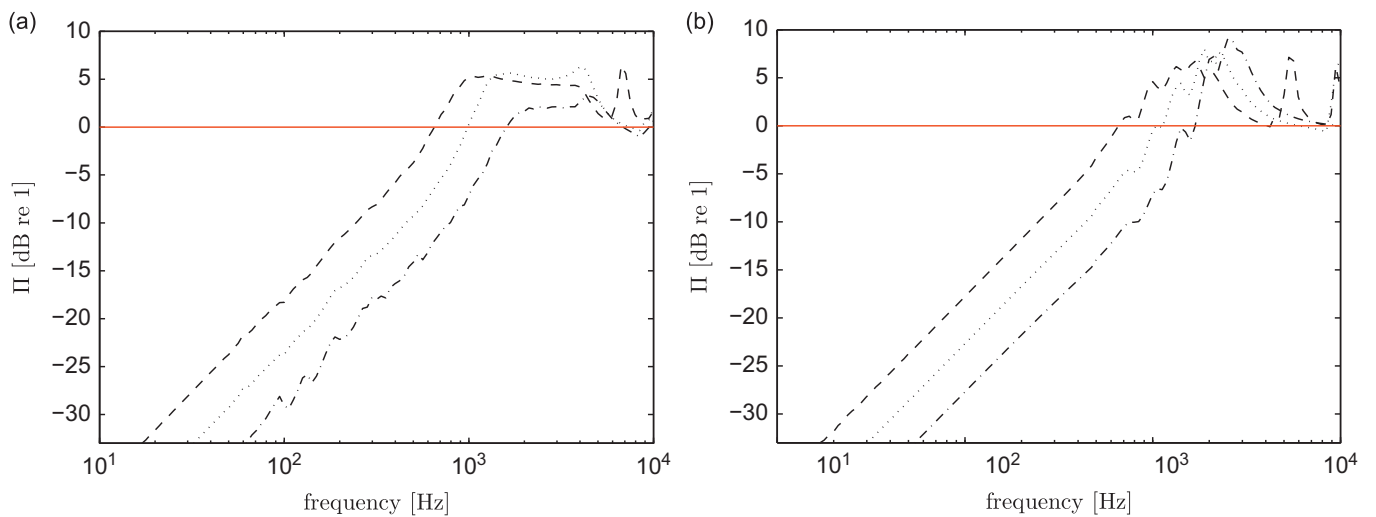

Fig. 9. Insertion gain due to the introduction of a rigid surface for radiated sound power of a perforated unbaffled plate: –, $D=40$ mm; $\cdots$, $D=20$ mm; $-\cdot-$, $D=10$ mm. Aluminium plate, $\eta=0.1$, $d_o=10$ mm, $\tau=10$ percent: (a) $0.65 \times 0.5 \times 0.003$ m and (b) $0.325 \times 0.25 \times 0.006$ m.
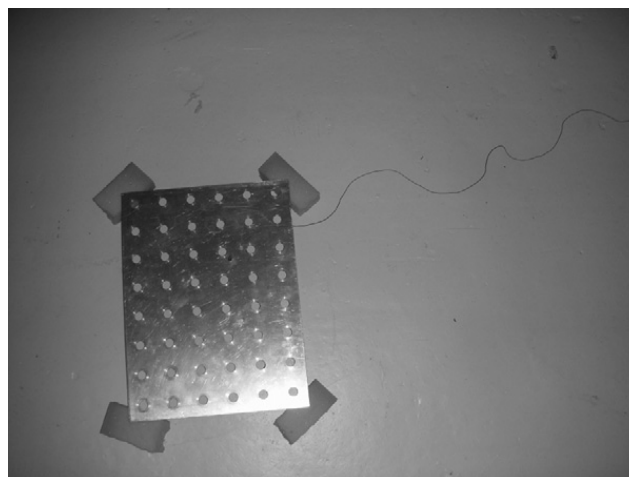

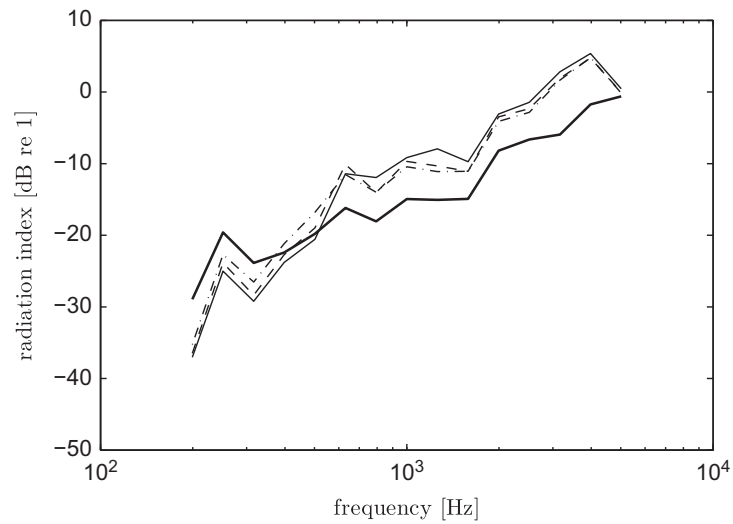**Fig. 10.** Arrangement of a perforated plate sample located close to the reverberation chamber floor.

Fig. 11. Measured radiation indices of a 3 mm aluminium solid plate near a rigid surface: absence of rigid surface (thick line), —, $D=10$ mm; –, $D=20$ mm; $-\cdot-$, $D=40$ mm.
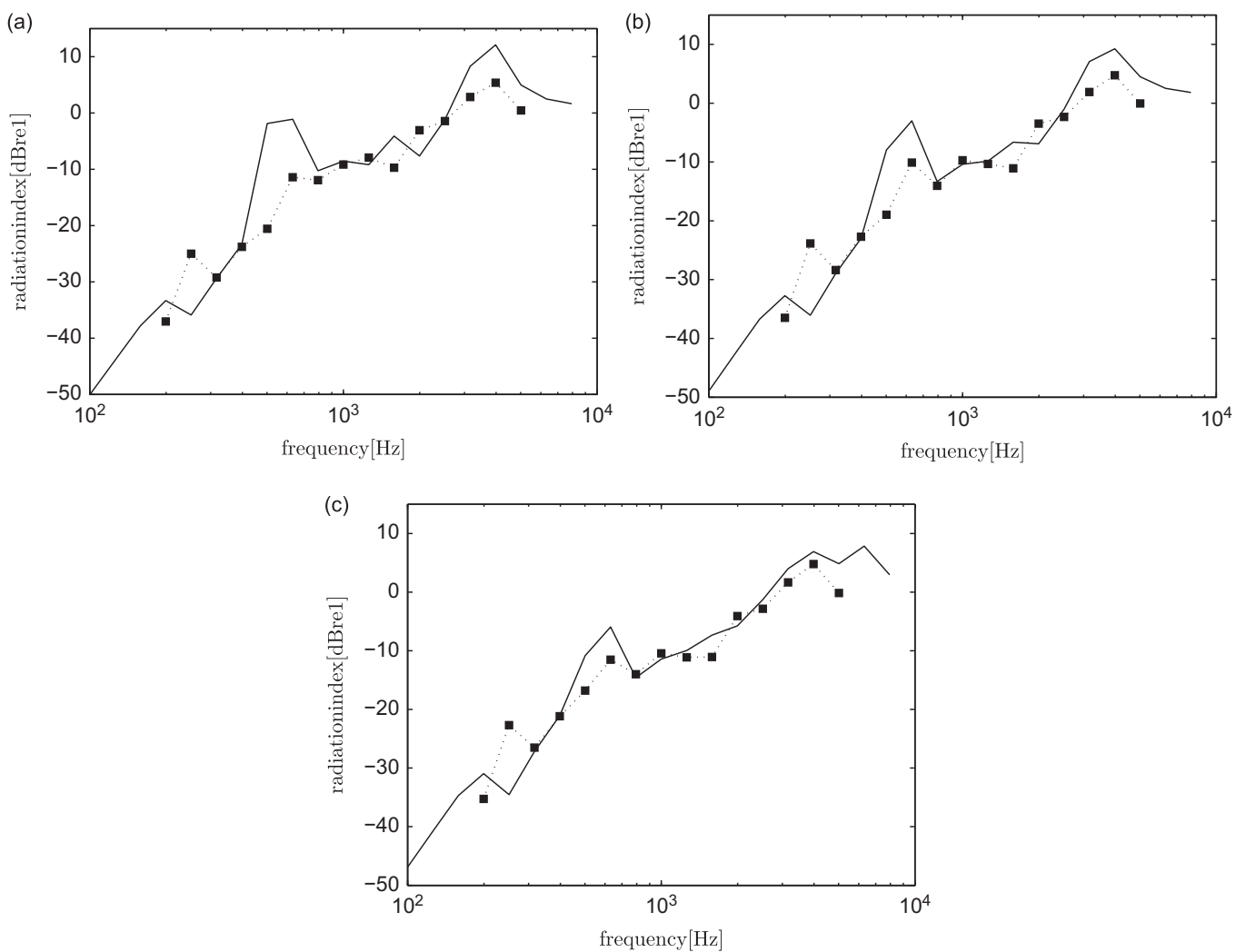

Fig. 12. Measured radiation indices of a 3 mm solid unbaffled plate near a rigid surface (■); —, theoretical; (a) $D=10$ mm, (b) $D=20$ mm and (c) $D=40$ mm.

results for the plate without the presence of a rigid surface, the plate was hung using soft ropes from a rigid frame. The distance from the bottom edge to the floor was around 1 m. As the plates were very lightly damped, adhesive damping patches were attached to parts of one side of all the plates to increase their damping. The damping loss factors for all the plates were found to be around $\eta = 0.01$ on average.

Clearly the experimental arrangement corresponds to free boundary conditions whereas the calculated results correspond to simply supported boundaries. However, it has been noted by Putra and Thompson [14] that the edge conditions have much less effect on the sound radiation for the case of an unbaffled plate than for a baffled plate.

The mechanical measurements were obtained in terms of transfer mobility with the plate excited by a shaker. The velocity was measured using a scanning laser vibrometer at 81 locations over the plate surface, while the excitation force was measured by a force transducer. A single force point was used, offset from the centre of the plate.

The acoustical measurement was conducted using a reciprocity technique in the reverberant chamber, where the plate was excited by a diffuse broadband sound field [15]. This technique was chosen to avoid noise from a shaker which could otherwise contaminate the measured sound power. The plate acceleration was measured by an accelerometer at the same point as the force was applied in the mobility measurement. The details of this method can be found in [15].

4.2. Measured results for solid plate

Fig. 11 shows the measured radiation indices ($10\log_{10}\sigma$) in one-third octave bands for the 3 mm aluminium plate having dimensions 0.4×0.3 m for different distances from the chamber floor. The results without the rigid surface are also plotted for comparison. The data are presented from 200 Hz as below this frequency the results are contaminated by background noise on the accelerometer signal due to the very low response at low frequencies. It can be seen that below about 600 Hz, the results are less than the measured result without the rigid surface and they decrease as the plate is
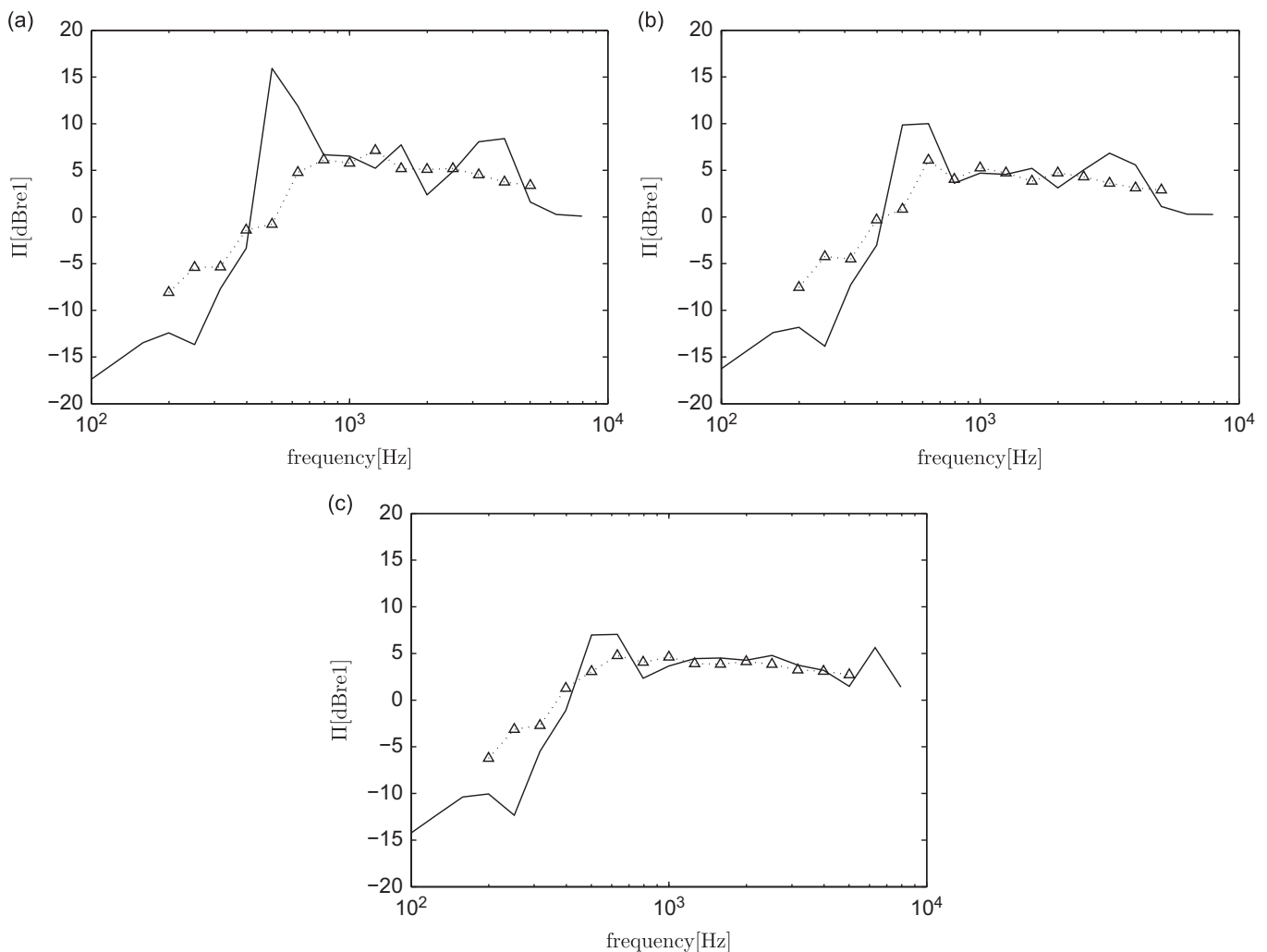

Fig. 13. Insertion gain due to the introduction of a rigid surface for radiated sound power of 3 mm solid unbaffled plates ($\triangle$); —, theoretical; (a) $D = 10$ mm, (b) $D = 20$ mm and (c) $D = 40$ mm.

located closer to the rigid surface. Above 600 Hz, the measured radiation efficiencies exceed that of the plate in the absence of the rigid surface. It can also be seen that in this region the result is increased as the distance from the surface is decreased. These findings are consistent with the theoretical results in Section 3.1 (see Fig. 3).

Fig. 12 shows a comparison between the measured results and the analytical calculation for this configuration. Good agreement is found despite the difference in boundary conditions. The measured results are also shown in the form of the insertion gain due to the rigid surface Π in Fig. 13. Again good agreement is found with the model, particularly above 1 kHz. It can be seen here that between 600 Hz and the critical frequency (4 kHz), the effect of the rigid surface is on average a gain of 5 dB, as found in the predictions. However, the peak in the predictions at 500 Hz, especially for $D=10$ mm is not found in the measurements.

4.3. Measured results for peforated plate

Fig. 14 shows the experimental results for a perforated 3 mm plate having 5 mm hole diameter and 20 percent perforation ratio. Results are shown for two distances from the rigid surface. The results agree well with the theoretical ones, also shown.

Fig. 15 plots results for perforated plates with thickness 1.5 mm and with different hole diameters and perforation ratios. It can be seen that the agreement between the measured radiation indices and the theoretical results, particularly at low frequencies, improves as the distance of the plate from the rigid surface increases (see also Fig. 14). This is due to the very low radiation efficiency of the perforated plate, where the results are more prone to influence by the noise floor of the instrumentation at low frequencies.

Fig. 16 shows examples of the measured insertion gains due to the rigid surface for perforated plates. For the three different distances of the sample plates from the rigid surface, good agreement can be seen between measurement and prediction above 1 kHz for the 1.5 mm thick plate and above 2 kHz for the 3 mm thick plate. As already mentioned, the
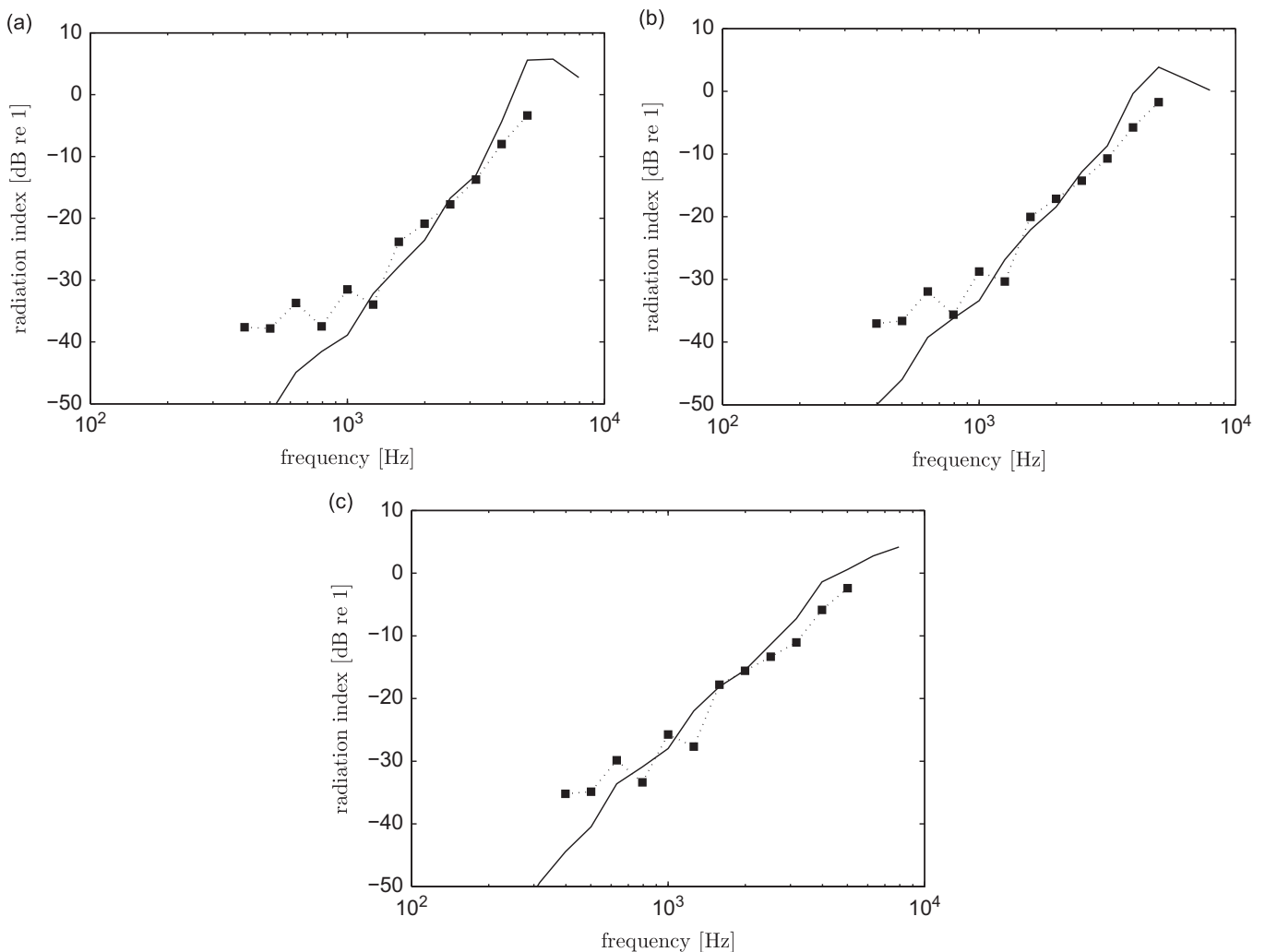

Fig. 14. Measured radiation indices of 3 mm perforated aluminium plates near a rigid surface (■) with $d_o=5$ mm, $\tau=20$ percent; —, theoretical; (a) $D=10$ mm, (b) $D=20$ mm and (c) $D=40$ mm.
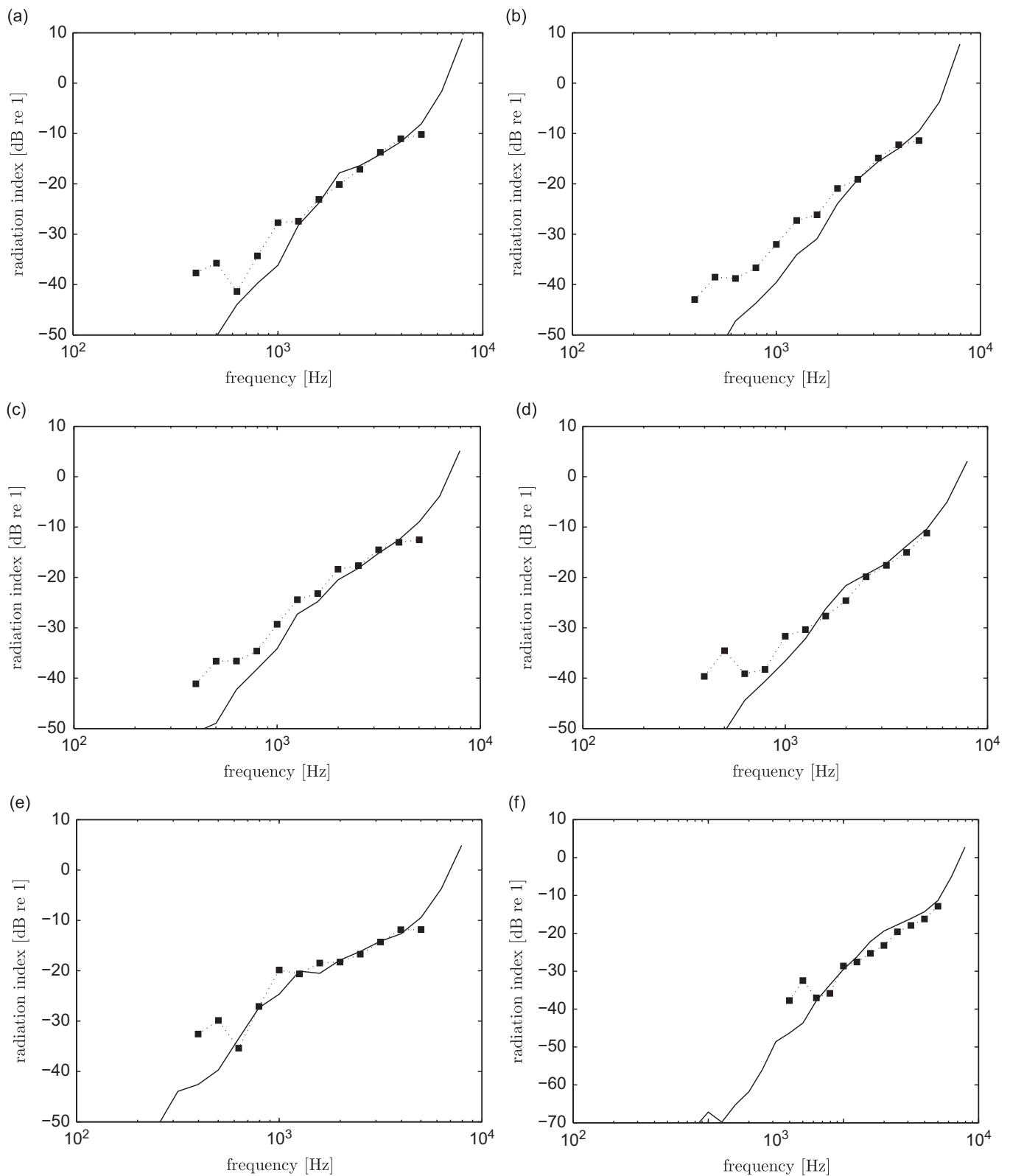
Fig. 15. Measured radiation indices of perforated 1.5 mm plates near a rigid surface (■): —, theoretical; $D=10$ mm: (a) $d_o=5$ mm, $\tau=5$ percent; (b) $d_o=8$ mm, $\tau=12$ percent, $D=20$ mm; (c) $d_o=8$ mm, $\tau=12$ percent; (d) $d_o=10$ mm, $\tau=19$ percent, $D=40$ mm; (e) $d_o=5$ mm, $\tau=5$ percent, (f) $d_o=10$ mm, $\tau=19$ percent.

discrepancies with the analytical calculation can be seen to be greater at low frequencies as the distance from the rigid surface becomes smaller (due to the accelerometer noise floor). Moreover, it is not easy to obtain a reliable result for the insertion gain because one has to deal with four input errors, i.e. from the sound power and the mobility measurements from plates both with and without the rigid surface.
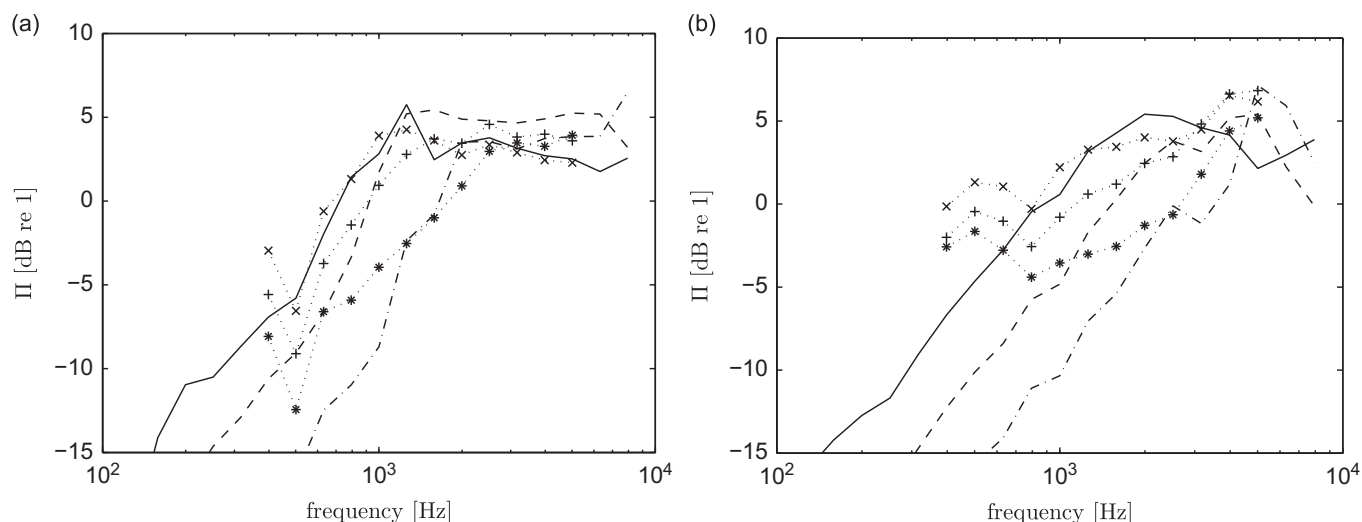
(a)

(b)

Fig. 16. Measured insertion gain due to the introduction of a rigid surface for an unbaffled perforated plate: (a) $t=1.5$ mm, $d_o=5$ mm, $\tau=5$ percent and (b) $t=3$ mm, $d_o=5$ mm, $\tau=20$ percent: ($*$)—, $D=10$ mm; ($+$)-, $D=20$ mm; ($\times$)– · –, $D=40$ mm (experiment, marked; theoretical, unmarked).

5. Conclusions

The sound radiation from an unbaffled plate close to a rigid surface has been calculated by extending Laulagnet's model for the radiation from an unbaffled plate [12]. To represent the presence of a reflecting rigid surface, an image source is introduced by modifying the Green's function in the model. The model is also extended for the case of a perforated plate by introducing the impedance of the holes, assuming it to be continuous over the plate surface.

It is found that the sound radiation is reduced considerably at low frequency when the plate is located close to a rigid surface at a distance much less than half the acoustic wavelength. This phenomenon can be used to reduce a predominantly low frequency noise from a thin source by positioning it near a rigid wall. By halving the distance to the rigid surface, the sound radiation only reduces by about 1 dB for the solid (unperforated) plate at these low frequencies. At higher frequencies, sharp peaks occur at the modal coincidence frequencies. These combine to give an amplification of the sound radiation which, on average, is about 5–6 dB for a separation distance of 10 mm. The amplification reduces as the distance from the rigid surface increases. Above the critical frequency the amplification is small apart from some peaks when the separation distance equals a multiple of half the acoustic wavelength.

Further reduction can be achieved by introducing perforation to the plate. This reduces the radiation for the unbaffled plate, but in addition the effect of introducing the rigid surface is found to be a considerable reduction at low frequencies. The radiation is still increased by the rigid surface in the mid frequency range but without the strong peaks found for the solid plate.

The model has also been validated by experiments which show a good agreement with the measured results both for the solid and perforated plates.

References

[1] L.E. Kinsler, A.R. Frey, A.B. Coppens, J.V. Sanders, *Fundamental of Acoustics*, fourth ed.,John Wiley & Sons, New York, 2000.
[2] G. Maidanik, Response of ribbed panels to reverberant acoustic fields, *Journal of the Acoustical Society of America* 34 (1962) 809–826.
[3] I.L. Vér, C.I. Holmer, Interaction of sound waves with solid structures, in: L.L. Beranek (Ed.), *Noise and Vibration Control*, McGraw-Hill, 1971 (Chapter 11).
[4] C.E. Wallace, Radiation resistance of a rectangular panel, *Journal of the Acoustical Society of America* 51 (1972) 946–952.
[5] F.G. Leppington, E.G. Broadbent, K.H. Heron, The acoustic radiation efficiency of rectangular panels, *Proceeding of the Royal Society London A* 382 (1982) 245–271.
[6] G. Xie, D.J. Thompson, C.J.C. Jones, The radiation efficiency of baffled plates and strips, *Journal of Sound and Vibration* 280 (2005) 181–209.
[7] V. Schroter, F.J. Fahy, Radiation from modes of a rectangular panel into a coupled fluid layer, *Journal of Sound and Vibration* 74 (1981) 575–587.
[8] J.W. Verheij, A.N.J. Hoeberichts, D.J. Thompson, Acoustical source strength characterization for heavy road vehicle engines in connection with pass-by noise, *Proceedings of 3rd International Conference on Recent Development in Air- and Structure-Borne Sound and Vibration*, Montreal, June 13–15, 1994.
[9] E.G. Williams, Numerical evaluation of the radiation from unbaffled, finite plates using the FFT, *Journal of the Acoustical Society of America* 74 (1983) 343–347.
[10] N. Atalla, J. Nicolas, C. Gauthier, Acoustic radiation of an unbaffled vibrating plate with general elastic boundary conditions, *Journal of the Acoustical Society of America* 99 (1996) 1484–1494.
[11] H. Nelisse, O. Beslin, J. Nicolas, A generalized approach for the acoustic radiation from a baffled or unbaffled plate with arbitrary boundary conditions, immersed in a light or heavy fluid, *Journal of Sound and Vibration* 211 (1998) 207–225.
[12] B. Laulagnet, Sound radiation by a simply supported unbaffled plate, *Journal of the Acoustical Society of America* 103 (1998) 2451–2462.
[13] E.G. Williams, J.D. Maynard, Numerical evaluation of the Rayleigh integral for planar radiators using the FFT, *Journal of the Acoustical Society of America* 72 (1982) 2020–2030.
[14] A. Putra, D.J. Thompson, Sound radiation from rectangular baffled and unbaffled plates, *Applied Acoustics* 71 (2010) 1113–1125.

[15] A. Putra, D.J. Thompson, Sound radiation from perforated plates, *Journal of Sound and Vibration* 329 (2010) 4227–4250.

[16] P.M. Morse, K.U. Ingard, *Theoretical Acoustics*, Princeton University Press, Princeton, NJ, 1986, pp. 366–370.

[17] F.J. Fahy, P. Gardonio, *Sound and Structural Vibration: Radiation, Transmission and Response*, second ed.,Academic Press, London, 2006.

[18] M.C.M. Wright, *Mathematics of Acoustics*, Imperial College Press, London, 2005.

[19] L. Cremer, M. Heckl, B.A.T. Petersson, *Structure-borne sound*, third ed.,Springer, Berlin, 2005.

[20] D. Takahashi, M. Tanaka, Flexural vibration of perforated plates and porous elastic materials under acoustic loading, *Journal of the Acoustical Society of America* 112 (2002) 1456–1464.

[21] D.Y. Maa, Microperforated panel wideband absorber, *Noise Control Engineering Journal* (November–December) (1987) 77–84.